SCIENCE CHINA
Physics, Mechanics & Astronomy

•Article•

August 2023 Vol. 66 No. 8: 286111
https://doi.org/10.1007/s11433-023-2121-2

The anelastic origin of mechanical cycling induced rejuvenation in the metallic glass

Langting Zhang[1], Yunjiang Wang[2,3], Yong Yang[4,5], and Jichao Qiao[1,6*]

[1]*School of Mechanics, Civil Engineering and Architecture, Northwestern Polytechnical University, Xi'an 710072, China;*
[2]*State Key Laboratory of Nonlinear Mechanics, Institute of Mechanics, Chinese Academy of Sciences, Beijing 100190, China;*
[3]*School of Engineering Science, University of Chinese Academy of Sciences, Beijing 100049, China;*
[4]*Department of Mechanical Engineering, College of Engineering, City University of Hong Kong, Hong Kong 999077, China;*
[5]*Department of Materials Science and Engineering, College of Engineering, City University of Hong Kong, Hong Kong 999077, China;*
[6]*Innovation Center, NPU-Chongqing, Chongqing 401135, China*

Received February 23, 2023; accepted April 19, 2023; published online July 6, 2023

Mechanical cycling is one of the effective methods to rejuvenate metallic glasses (MGs) and improve their mechanical properties. The anelastic origin of the rejuvenation by mechanical cycling in a $La_{30}Ce_{30}Ni_{10}Al_{20}Co_{10}$ MG was investigated via differential scanning calorimetry (DSC) and dynamic mechanical analysis (DMA). We demonstrate that mechanical cycling promotes the activation of flow defects with short relaxation times, leading to anelastic strains and therefore considerable energy storage, which manifests itself as larger relaxation enthalpy on the DSC curves of MGs. However, the MGs release the excess relaxation enthalpy caused by anelastic strain with time, thus suppressing atomic mobility and elevating β relaxation activation energies. The strategy of mechanical cycling at small strains, as demonstrated in the current work, can expand the energy states of MGs over a wide range of relaxation enthalpies.

metallic glass, mechanical cycling, rejuvenation, anelastic strain, structural heterogeneity

PACS number(s): 61.43.Dq, 62.40.+i, 62.20.Hg

Citation: L. Zhang, Y. Wang, Y. Yang, and J. Qiao, The anelastic origin of mechanical cycling induced rejuvenation in the metallic glass, Sci. China-Phys. Mech. Astron. **66**, 286111 (2023), https://doi.org/10.1007/s11433-023-2121-2

1 Introduction

Metallic glasses (MGs) possess unique mechanical properties and are considered as ideal structural materials [1,2]. The little macroscopic plasticity restricts their practical applications due to the formation of shear bands [3]. The energetic state of MGs is dependent on the external temperature history and spontaneously ages with time once they are prepared [4,5]. Generally speaking, higher cooling rates drive MGs trapped in more energetically unstable configurations in the potential energy landscape (PEL) with more heterogenous structure and larger fraction of flow defects than lower rates [6,7]. Upon successive structural relaxation processes, MGs continually explore different configurations until they age towards energetically stable configuration in the PEL. This spontaneous process is called physical aging and changes the structural, thermal, and mechanical properties of MGs [8]. In stark contrast, the rejuvenation process drives MGs into energetically unstable configurations, which is analogous to quenched MGs theoretically obtainable with cooling rates in some cases [9,10].

Amounts of thermomechanical strategies have been proposed to achieve the rejuvenation [11-14]. Significantly, strategies within the nominal elastic limit (such as cryogenic

*Corresponding author (email: qjczy@nwpu.edu.cn)

thermal cycling, mechanical cycling, and elastostatic loading) are of abundant attention in exploring the underlying mechanisms acting in MGs undergoing externally thermo-mechanical stimuli [15-17]. Mechanical cycling is of particular interest: homogenous at tailoring the microstructure, easy to operate and efficient at achieving the high-energy state. The degree of rejuvenation depends on the initial state of the glass, and on processing parameters, i.e., cycling temperature, frequency, and amplitude [18]. These flexibilities give valuable freedom in designing the mechanical cycling processing [19]. However, the coupling of anelastic and plastic deformation, and a competition between structural relaxation and rejuvenation in mechanical strategies have been continuedly argued [17,20]. It is necessary to clarify what role each strain component takes and how they affect the mechanical properties of MGs, considering the time elapsed after mechanical cycling.

Though the practical interests focus more on improving the mechanical properties of MGs, the excess energy stored in the glassy system by these strategies is the most pivotal quantitative index to the level of rejuvenation. Our results confirm the availability of rejuvenation by mechanical cycling within the nominal elastic limit. The anelastic origin of the energy store is examined by differential scanning calorimetry (DSC) and dynamic mechanical analysis (DMA). Discrete relaxation spectrum is constructed to describe the distribution of flow defects during the anelastic deformation. The work done (WD) by mechanical cycling is only several tenths of the stored energy in our glass, which suggests that anelastic strain introduces an endothermic process and draws heat into the glassy system. The core results provide an essential piece for extending the range of the glassy state and shed vital light on the mechanical rejuvenation.

2 Experimental procedure

$La_{30}Ce_{30}Ni_{10}Al_{20}Co_{10}$ (at%) MG [21] were prepared by single-roller melt-spinning in an argon atmosphere into ribbons with a width of 1.2 mm and a thickness of 30 μm. Thermal analysis was carried out by differential scanning calorimeter (Netzsch DSC 404 F3) at a heating rate of 20 K/min under high-purity argon flow. The mechanical cycling, strain recovery, and dynamic mechanical behavior experiments were performed using the commercial dynamic mechanical analyzer (TA Q800) in tensile mode. The cycling temperature was isothermal for 10 min to confirm thermal equilibration before the mechanical cycling and pre-tension load of 0.01 N was employed to reduce the bending of ribbons during isothermal processes.

Figure 1(a) displays the protocol of mechanical cycling and strain recovery at 365 K below the glass transition temperature T_g (~438 K). During the recovery process, the elastic strain ε_e instantaneously recovers, anelastic strain ε_{an} recovers with time, and viscoplastic strain ε_{vp} that cannot recover. The mechanical cycling was carried out in three modes: (1) at constant stress rate of 50 MPa/min and mean stress of 100 MPa, the stress amplitude ranges from 0 to 200 MPa; (2) at mean stress of 100 MPa and amplitude of 100 MPa, the stress rate ranges from 12.5 to 200 MPa/min; (3) at constant stress rate of 50 MPa/min and amplitude of corresponding mean stress, the mean stress ranges from 25 to 200 MPa. These modes were repeated for 8 h for one complete set of cycle.

3 Results and discussion

Figure 1(b)-(d) exhibit the strain evolution during the mechanical cycling and recovery processes at different stress rate, mean stress, and stress amplitude, respectively. These curves are similar to that of traditional glassy creep [22]. The initial stage of strain is called primary creep, which is characterized by a gradual increase followed by an approximate saturation. The steady-state creep is a period that strains linearly and increases with time. The creep intensity of these two stages shows a strong dependence on mechanical cycling intensity. Increasing the mechanical cycling intensity sharply accelerates the creep process, which is confirmed by the gradual increase of the strain and strain rate. Yang's group [23] proposed a "core-shell" model, i.e., soft regions and their surrounding elastic matrix, to describe the heterogeneous microstructure of MGs. These soft regions with relatively high atomic mobility are easier to be activated, undergoing external stress. We suggest that the flow defects in glassy ribbons can be activated even at an external stress far less than their yield limit. In such a case, mechanical cycling is helpful to promote the transition from atoms in the glassy matrix to soft regions. As for the recovery process, the total strain decreases with recovery time but increases with mechanical cycling intensity. For a more intuitive perspective, the initial and final strains during recovery processes at various mechanical cycling technologies are shown in Figure 1(e) to study the strain recovery intensity. The difference corresponds to the local anelastic strain in the experimental window. We have seen that the residual or viscous-plastic strain progressively increases with mechanical cycling intensity, which suggests a decrease in flow viscosity. The increase of anelastic strain increases with loading time or cycling intensity, demonstrating a promotion of activation of flow defects and accumulating of the local plastic flow.

The heterogenous microstructure of MGs leads to the complexity and mystery of high-temperature flow. A great deal of effort has been made to explain the correlation between phenomenological flow and non-Debye relaxation

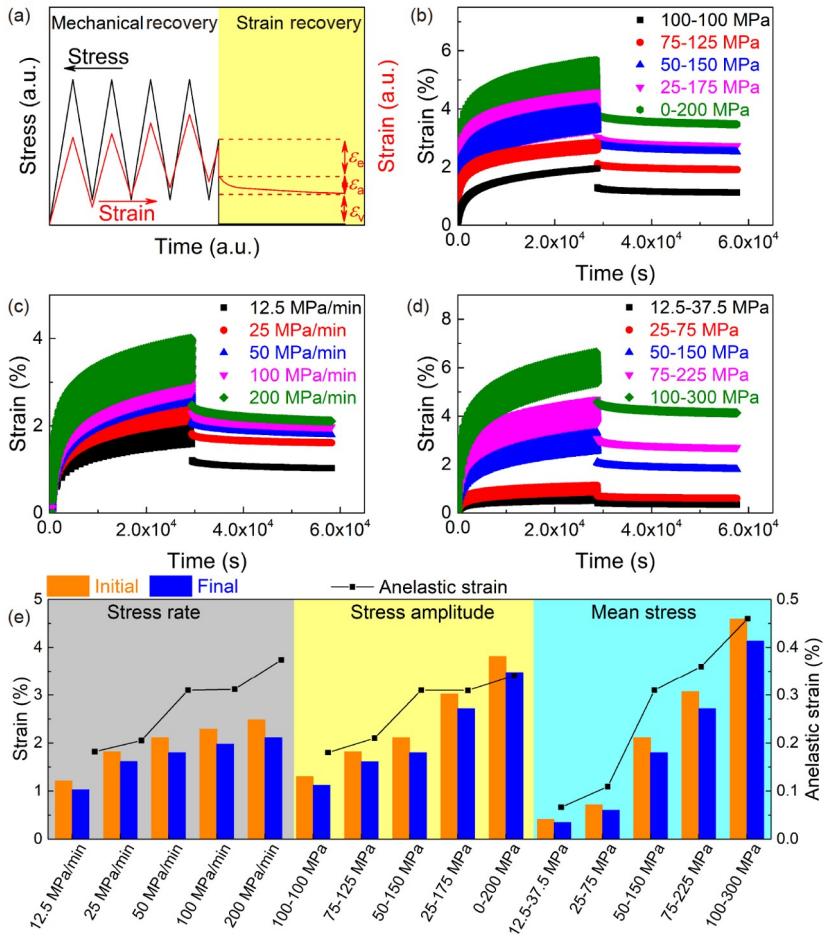

Figure 1 (Color online) (a) Schematic diagram of evolution of stress and strain on time during mechanical cycling and strain recovery experiments. ε_e is the instantaneous reversible elastic strain, ε_{an} is the anelastic strain that recovers with time, and ε_{vp} is irreversible visco-plastic strain. (b)-(d) Time dependence of strain during mechanical cycling and strain recovery process at different stress amplitudes, stress rates, and mean stresses, respectively. (e) Evolution of initial, final, and anelastic strain on cycling method.

dynamics [24,25]. Let us consider that high-temperature flow in MGs is originally due to local stress-assisted, thermally activated shear transformations through cooperative atomic rearrangements. The characteristic relaxation time of a shear event is τ_1. The activated shear event either returns toward the initial configuration when unloading or gets de-activated because of structural relaxation and plastic deformation. The characteristic relaxation time of this process is τ_2. As for a homogenous structure, the deformation can be described by the activation and de-activation of shear events. There should be a dynamic balance between these two configurations undergoing external stress: a population transition of regions between the activated state to the de-activated state. Thus, the following equation is established to describe the creep and recovery processes:

$$\begin{cases} \varepsilon_{\text{creep}} = \varepsilon_{\text{e}} + \varepsilon_{\text{an}}\left[1-\exp\left(-\dfrac{t}{\tau}\right)\right] + \dot{\varepsilon}_{\text{vp}}t, \\ \varepsilon_{\text{recovery}} = \varepsilon_{\text{an}}\left[1-\exp\left(\dfrac{t_0}{\tau}\right)\right]\exp\left(\dfrac{t_0-t}{\tau}\right) + \dot{\varepsilon}_{\text{vp}}t_0, \end{cases} \tag{1}$$

with stress=σ for $0 \leqslant t \leqslant t_0$ and stress=0 for $t > t_0$. Here $1/\tau = 1/\tau_1 + 1/\tau_2$. Because of the disordered atomic rearrangements in MGs, a single value of the relaxation time is no longer appropriate to describe the distribution of flow defects. Lei et al. [26] suggested the relaxation time of flow defects involving deformation even over eleven orders of magnitude of time. A generalized Kelvin model composed of a series of linear springs and dashpots is used to describe the distribution of discrete relaxation times during creep and recovery processes as:

$$\begin{cases} \varepsilon_{\text{creep}} = \varepsilon_{\text{e}} + \sum_{i=1}^{n} \varepsilon_{\text{an\_}i}\left[1-\exp\left(-\dfrac{t}{\tau_i}\right)\right] + \dot{\varepsilon}_{\text{vp}}t, \\ \varepsilon_{\text{recovery}} = \sum_{i=1}^{n} \varepsilon_{\text{an\_}i}\left[1-\exp\left(-\dfrac{t_0}{\tau_i}\right)\right]\exp\left(\dfrac{t_0-t}{\tau_i}\right) + \dot{\varepsilon}_{\text{vp}}t_0. \end{cases} \tag{2}$$

Here $1/\tau_i = 1/\tau_{1\_i} + 1/\tau_{2\_i}$, τ_{1_i} and τ_{2_i} are the relaxation time of activation and deactivation of i-type shear event. The relaxation time values, τ_i, i=1, …, n=60 (n should be less than the data point number), are logarithmically spaced in the

range of relaxation times between 10^{-2} and 10^{8} s. The regularization term was used in the optimization procedure to avoid overfitting. The calculation of relaxation time distribution is sensitive to small differences in experimental data. The repeatability of mechanical cycling experiments has been checked before the calculation (as shown in Figure S1(a), Supporting Information online). A regularization parameter that is too large will lead to underfitting but too small will lead to overfitting. The spectrum exhibits a negligible change within an applicable range of regularization parameter values (as shown in Figure S1(b)). The regularization parameter value was chosen as 0.1 for all curves. The best fitting of strain recovery at stress amplitude of 0-200, 50-150, and 100-100 MPa are shown in Figure 2(a). The characteristic relaxation time distribution at various stress rates and mean stresses are shown in Figure S1(c) and (d). Compared with pure creep (100-100 MPa), increasing stress amplitude introduces an increase of anelastic and viscoplastic strain. Only a fraction of the total anelastic strain gets recovery in the experimental window. We can see that the anelastic strain totally recovers at about 10^{8} s. The evolution of strain recovery at a longer time is dependent on their prior cycling technology, i.e., samples with higher cycling intensity possess larger strain that recovers faster. The anelastic process with a large relaxation time can be accelerated during a much shorter time by higher cycling intensity. Figure 2(b) displays the discrete relaxation-time spectra computed from Figure 2(a), shifted vertically for an intuitive perspective. All spectra show various distinct peaks, which are correlated to distinct flow defect types. The peak times shift to shorter time region and their intensity increases, especially at peak times less than 10^{4} s with increasing cycling intensity. The first two peaks in the spectra of sample

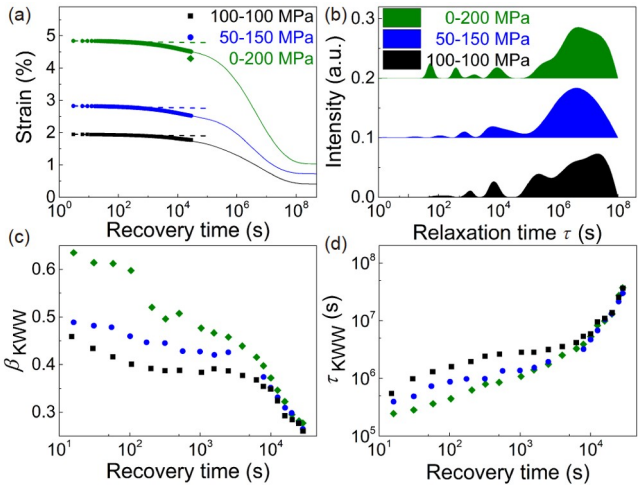

Figure 2 (Color online) Samples at various stress amplitudes. (a) Evolution of strain with time during the recovery process. The solid lines were fitting by eq. (2). (b) Characteristic relaxation time distribution. The calculated instant (c) extended exponent β_{KWW} and (d) characteristic relaxation time τ_{KWW} as a function of recovery time.

"0-200 MPa" are the most distinct compared with that of others. Thus, we speculate that mechanical cycling is beneficial to activate flow defects with a short relaxation time.

To level the degree of dynamic heterogeneity during the recovery process, an empirical stretched exponential Kohlrausch-Williams-Watts (KWW) function is used by rewriting eq. (2) as [27]:

$$\varepsilon(t) = \varepsilon_{\mathrm{an}} \exp\left(-\frac{t}{\tau_{\mathrm{KWW}}}\right)^{\beta_{\mathrm{KWW}}} + \varepsilon_{\mathrm{vp}}, \tag{3}$$

where KWW is the characteristic time of the recovery process; β_{KWW} is the stretched parameter, which is closely correlated to the structural heterogeneity of glassy systems. Interestingly, Gao et al. [28] took a double logarithm on both sides of the KWW equation to characterize the instant relaxation kinetics. Here we would focus on instant dynamic heterogeneity in the recovery process. The eq. (3) can be rewritten as $\ln\left[\ln\left(\frac{\varepsilon_{\mathrm{an}}(0)}{\varepsilon_{\mathrm{an}}(t)}\right)\right] = \beta_{\mathrm{KWW}}[\ln(t) - \ln(\tau_{\mathrm{KWW}})]$. The evolution of instant values of β_{KWW} and KWW on recovery time at various cycling technology can be readily computed, as shown in Figure 2(c) and (d). The instant β_{KWW} decreases but instant τ_{KWW} increases with the recovery time for all cycling technology, which shows that the relaxation dynamics are more heterogeneous but slower with the recovery time. Obviously, the β_{KWW} value of sample "0-200 MPa" is higher than others while the τ_{KWW} value is the shortest, denoting that mechanical cycling induces a more intense, faster and homogenous anelastic deformation into MGs. At about 10^{4} s, the instant β_{KWW} and τ_{KWW} values trace almost identical paths. It agrees with the distribution of discrete relaxation times in Figure 2(b), as indicating by the intensity and peak time at relaxation time those are lower than 10^{4} s. It is evident that increasing the mechanical cycling intensity is beneficial to accelerate the activation of soft regions with relaxation time less than 10^{4} s, rather than the glassy matrix with longer relaxation time. Taking consideration of our previous work of rejuvenation by mechanical cycling [15], these results are also beneficial to clarifying the correlation between rejuvenation and anelastic strain.

The variation of the internal energy of any closed systems with constant volume is the sum of the input mechanical energy and their adsorbed thermal energy. However, there are local shear transformations that are not totally reversible at puny strains well within the elastic region of MGs, i.e., atomic configurations are not recovered while the sample returns to its original macroscopical dimensions [29]. The competition between the stored energy by inelastic strain and the dissipated energy by structural relaxation determines the direction of rejuvenation or aging. The mechanical energy or work done is totally contributed by pure creep at a stress ratio $\sigma_{\max}/\sigma_{\min}$ of 1.0 while by pure cycling at a stress ratio $\sigma_{\max}/\sigma_{\min}$

of −1.0. Generally, the work done in mechanical cycling is the sum of components of pure creep and pure cyclic loading as:

$$\begin{aligned} &\upsilon_{\text{total}} = \upsilon_{\text{creep}} + \upsilon_{\text{cycling}} / 2, \\ &\upsilon_{\text{creep}} = \sigma\varepsilon_{\text{creep}}, \\ &\upsilon_{\text{cycling}} = \sum_{i=1}^{n} \upsilon_{\text{cycling\_}i}, \end{aligned} \tag{4}$$

where υ_{total}, υ_{creep}, and $\upsilon_{\text{cycling}}$ are total, creep, cycling strain energy densities, respectively, $\upsilon_{\text{cycling\_}i}$ is the hysteresis area per cycle for the i-th cycle, and $\varepsilon_{\text{creep}}$ is equal to $\left(\varepsilon_{\text{max\_cycle}} + \varepsilon_{\text{min\_cycle}}\right)/2$. $\varepsilon_{\text{max\_cycle}}$ and $\varepsilon_{\text{min\_cycle}}$ are the maximum and minimum strain values per cycle. Based on eq. (4), the evolution of υ_{total} on cycling time at various stress amplitudes can be readily computed, as shown in Figure 3(a). The results show that υ_{total} monotonously increases with cycling time, while their increase rate gradually decreases towards a constant. Reasonable trend displays $\upsilon_{\text{cycling}}$ takes a more vital role in contributing to υ_{total}, which suggests a higher fraction of work done by cycling deformation. Both literatures have reported a rejuvenation by mechanical cycling at room temperature and relatively high temperature [15,30], although no further information about the effect of strain recovery was provided. One can compute the recovery time evolution of anelastic υ_{an}, visco-plastic υ_{vp}, and dissipated υ_{diss}components as:

$$\begin{aligned} &\upsilon_{\text{total}}(t) = \upsilon_{\text{an}}(t) + \upsilon_{\text{vp}} + \upsilon_{\text{diss}}, \\ &\upsilon_{\text{an}}(t) = \sigma_{\text{creep}}\varepsilon_{\text{an}}, \\ &\upsilon_{\text{vp}}(t) = \sigma_{\text{creep}}\varepsilon_{\text{vp}}, \\ &\upsilon_{\text{diss}} = \upsilon_{\text{cycling}} / 2 = \sum_{i=1}^{n} \upsilon_{\text{cycling\_}i} / 2, \end{aligned} \tag{5}$$

where σ_{creep} is equal to $\left(\sigma_{\text{max\_cycle}} + \sigma_{\text{min\_cycle}}\right)/2$. Taking sample "0-200 MPa" as an example, the work done evolution during the mechanical cycling and recovery processes is calculated, as shown in Figure 3(b). These components during the recovery process are quantificationally decoupled based on Figure 2(a). The dissipated component is competed against the structural relaxation and promotes the disorder. At first glance, only a fraction of υ_{total} gets recovery. To study the effect of strain recovery, the recovery times of the DSC and DMA tests are marked in Figure 3(b) with blue stars.

As-cast glasses give a heat release near the glass transition when they are heated at a rate lower than their forming cooling rate [31]. The relaxation enthalpy ΔH is the most effective quantification of the energetic state of MGs. Figure 4 shows the heat flow difference between glassy samples and their crystallized counterparts. The shape of the exothermal peak on the DSC spectrum is dependent on the heating rate, obeying a Kissinger activation energy [32]. In order to facilitate comparison, a standard heating rate of 20 K/min was carried out. The ΔH value increases from 0.34 to 0.79 kJ/mol

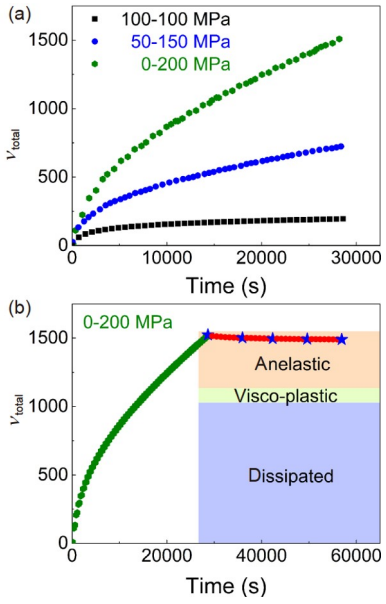

Figure 3 (Color online) (a) Cycling time dependence of υ_{total} at various stress amplitudes; (b) evolution of υ_{total} in the sample "0-200 MPa" during mechanical cycling and strain recovery processes.

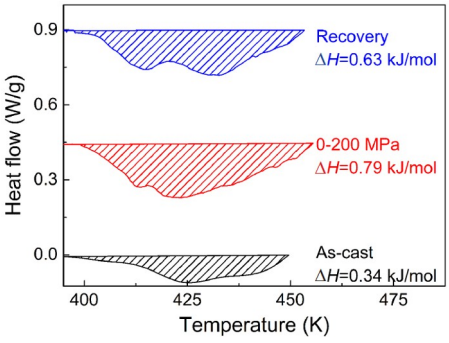

Figure 4 (Color online) DSC curves of glassy samples. The relaxation enthalpy ΔH increases with the mechanical cycling and then decreases because of the recovery of anelastic strain.

after mechanical cycling of 0-200 MPa but decreases to 0.63 kJ/mol after 8-hour recovery. The value of increase of ΔH is 0.45 kJ/mol and higher than the La-based ribbon rejuvenated by thermal cycling (~0.37 kJ/mol) [9]. Mechanical cycling allows straightforward calculation of the WD based on dimension, mass and strain energy per unit volume of the sample as $\text{WD} = \frac{\upsilon_{\text{total}} V}{M}$, where V is the volume of glassy ribbon and M is the molar mass. We gave the WD value of sample "0-200 MPa" as 4.4×10^{-2} kJ/mol. Evidently, the stored energy in MGs (~0.45 kJ/mol) exceeds the mechanical WD. This is interesting since the common concept is that the stored energy in only a fraction of the WD is no more supportable. Some other results about mechanical rejuvenation and $\Delta(\Delta H)$/WD value are summarized and shown in Table 1 (the results are directly computed or conservatively esti-

Table 1 The $\Delta(\Delta H)$/WD value in different mechanical strategies. The results are directly computed or conservatively estimated from the original literatures

Glass	Method	Temperature	$\Delta(\Delta H)$/WD	Ref.
$Cu_{65}Zr_{35}$	elastostatic loading	RT	2.55	[33]
$Ni_{62}Nb_{38}$	elastostatic loading	RT	1.87	[34]
$Cu_{65}Zr_{35}$	elastostatic loading	RT	5.66	[35]
$Cu_{50}Zr_{50}$	elastostatic loading	RT	7.41	[36]
$Pd_{40}Cu_{30}Ni_{10}P_{20}$	shot-peening	RT	5.7%-7.4%	[37]
$Pd_{77.5}Cu_6Si_{16.5}$	cold rolling	RT	<10%	[38]
$Zr_{57}Ti_5Cu_{20}Al_{10}Ni_8$	high pressure torsion	RT	<20%	[39]
$La_{30}Ce_{30}Ni_{10}Al_{10}Co_{20}$	mechanical cycling	0.83 T_g	10.01	current work

mated from the original refs. [33-39]). A series of points can be proposed after checking energy values in different technologies. The most apparent difference between these rejuvenation strategies is the temperature and the degree of deformation. Heavy plastic deformation, i.e., shot-peening, cold rolling, and high-pressure torsion, at room temperature (RT) all exhibit a traditional efficiency that $\Delta(\Delta H)$/WD<1. The operation of shear bands can induce considerable temperature excursions, which rises by thousands of degrees for nanoseconds [40], and it is therefore not surprising that the majority of WD dissipates in the form of heat. In contrast, it is remarkable that mild technologies, i.e., mechanical cycling and elastostatic loading, as loading in the elastic regime can introduce slight deformation and extraordinary efficiency that $\Delta(\Delta H)$/WD>1, which indicates these processes should be considered to be spontaneous rather than driven. The stored energy efficiency of mechanical cycling at 0.83 T_g is apparently higher than that of elastostatic loading at RT; one can draw a conclusion that the mechanical cycling in the β relaxation temperature region (see below) is more effective to store energy and rejuvenate MGs.

Now the challenge is to understand how mechanical cycling can lead to disordering. We suggest that mechanical cycling creates an endothermic process, absorbing heat from the surroundings into the sample. Mechanical cycling was carried out isothermally, thus, the temperature increase should be arbitrarily small, and the heat energy rapidly drives samples to transform into a higher degree of disorder. In this case, mechanical cycling is more like a high-performance catalyst that promotes these endothermic processes (analogous to the non-affine strain in thermal cycling [9]). The new configuration possesses higher enthalpy and entropy and becomes heterogenous. In fact, the shear-induced melting and disordering in some glassy systems have been previously reported [41], which is in parallel with MGs [18]. Reviewed the evolution of v_{total} during the recovery in Figure 3(b), the recovery energy value of anelastic strain is 1×10^{-3} kJ/mol while the $\Delta(\Delta H)$ value with 8-hour recovery is 0.16 kJ/mol. If we ignore the continuous structural relaxation during the recovery process, the recovery anelastic strain stores energy which is even equivalent to 160 times of itself. This degree is unreasonably large because of the more severe spontaneous structural relaxation in more heterogenous MGs. If we further assume that rejuvenation is induced by anelastic strain rather than visco-plastic strain, a more reasonable ratio between the stored energy in anelastic strain and itself can be obtained as 16. The energy storage efficiency of about dozens of times suggests that the rejuvenation induced by mechanical cycling is mainly attributed to the anelastic strain, which is particularly correlated to the endothermic process.

The evolution of the exothermal peak with the structural state on the DSC spectrum is similar to that of the loss modulus lying on the dynamic mechanical spectrum. The β relaxation of MGs exhibits various types, i.e., "peak", "shoulder", and "excess wing", depending on the chemical composition [2,42]. The temperature dependence of loss factor tanδ at various recovery times is represented in Figure 5(a). The frequency is 1 Hz and heating rate is 2 K/min. The data of the as-cast sample is also included as a reference. Obviously, the recovery anelastic strain releases the stored mechanical energy in the glassy system and consequently, the β relaxation intensity decreases and shifts toward the high-temperature region with the recovery time, which indicates a feature of structural de-rejuvenation and agrees with the decrease of ΔH in Figure 4. One can observe that the β relaxation intensity in samples with various recovery times is still higher than that of as-cast glass, which demonstrates the pretty sustainability of rejuvenation by introducing the anelastic strain. Compared with other strategies, mechanical cycling is remarkable to strengthen the β relaxation and to extend the range of the glassy state [6]. The anelastic recovery couples with physical aging during the recovery process. It is necessary to disentangle the contribution of pure aging from the effect of anelastic recovery. Temperature dependence of loss factor tanδ with various thermal-mechanical histories is shown in Figure S2. Additionally, the relative change of peak temperature and loss factor intensity are calculated and shown in Table S1 (Supporting Information online). Compared with pure aging, the strain recovery introduces a more apparent change in peak temperature and loss factor intensity. Consequently, the de-rejuvenation during the recovery process is more to be attributed to the an-

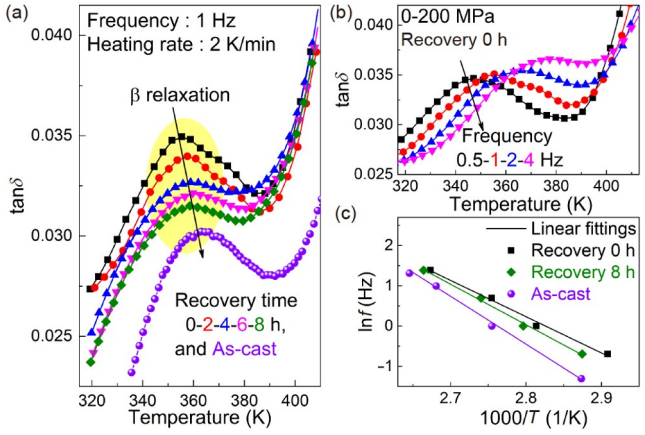

Figure 5 (Color online) Effect of anelastic strain on rejuvenation. (a) Temperature dependence of loss factor tanδ at various recovery times. The data of the as-cast sample is included as reference; (b) frequency dependence of loss factor tanδ of sample "0-200 MPa"; (c) the Arrhenius plot of frequency versus temperature. Solid lines are the best fits by eq. (5).

elastic recovery rather than standard physical aging.

Figure 5(b) gives the temperature dependence of loss factor tanδ at driving frequencies f (1-2-4-8 Hz) and at a heating rate of 2 K/min. The β relaxation peak temperature increases with the frequency and their internal correlation obeys an Arrhenius equation as $f = f_0 \exp\left(-E_\beta / k_B T\right)$, where f_0 is a pre-parameter, E_β is the apparent β relaxation activation energy, and k_B is the Boltzmann constant. The β relaxation activation energy with various recovery times was computed based on eq. (5) as shown in Figure 5(c). The data of the as-cast sample is included as ref. [15]. Compared with the as-cast MG (E_β=0.92 eV), the E_β value firstly decreases to 0.73 eV after mechanical cycling and then increases to 0.82 eV after 8 h recovery. The non-monotonic evolution of β relaxation activation energy during the mechanical cycling and recovery processes follows the trace of anelastic strain. The stored energy increases with the accumulation of anelastic strain, but decreases with recovery of that.

The correlation between rejuvenation and anelastic deformation has been hinted at in our or other previous studies [43-46]. Our results confirm that the rejuvenation by flow originated from the endothermic process induced by anelastic strain rather than mechanical energy stored in itself. Significantly, the greatest challenge is how to retain these anelastic strains or heat to the maximum extent from the experimental and simulated perspectives.

4 Conclusions

In summary, the mechanical cycling below the T_g can lead to rejuvenation in a $La_{30}Ce_{30}Ni_{10}Al_{10}Co_{20}$ MG. We give the anelastic origin of the rejuvenation through our strategy via differential scanning calorimetry and dynamic mechanical analysis. Increasing the mechanical cycling intensity can effectively activate flow defects with a short relaxation time and promote the transition of atoms in the glassy matrix to flow defects, which strengthens the accumulation of anelastic strain. Interestingly, we find that the stored energy characterized by structural enthalpy exceeds the work done on glassy samples by a factor of dozens of times. The considerable energy storage efficiency is mainly attributed to the anelastic strain, which is correlated to the endothermic process. During the strain recovery process, $La_{30}Ce_{30}Ni_{10}Al_{10}Co_{20}$ MG releases the excess relaxation enthalpy with the recovery time and gets de-rejuvenation, which suppresses the atomic mobility and increases the β relaxation activation energy.

This work was supported by the National Natural Science Foundation of China (Grant Nos. 51971178, and 52271153), the Natural Science Basic Research Plan for Distinguished Young Scholars in Shaanxi Province (Grant No. 2021JC-12), the Fundamental Research Funds for the Central Universities (Grant No. D5000220034), and the Natural Science Foundation of Chongqing (Grant No. cstc2020jcyj-jqX0001). Yunjiang Wang was supported by the National Natural Science Foundation of China (Grant No. 12072344), and the Youth Innovation Promotion Association of the Chinese Academy of Sciences. Yong Yang acknowledges support from the Research Grant Council (RGC), and the Hong Kong government through the General Research Fund (GRF) (Grant Nos. CityU11200719, and CityU11213118).

Supporting Information

The supporting information is available online at http://phys.scichina.com and https://link.springer.com. The supporting materials are published as submitted, without typesetting or editing. The responsibility for scientific accuracy and content remains entirely with the authors.

1 J. C. Qiao, Q. Wang, J. M. Pelletier, H. Kato, R. Casalini, D. Crespo, E. Pineda, Y. Yao, and Y. Yang, Prog. Mater. Sci. **104**, 250 (2019).
2 W. H. Wang, Prog. Mater. Sci. **106**, 100561 (2019).
3 A. L. Greer, Y. Q. Cheng, and E. Ma, Mater. Sci. Eng.-R-Rep. **74**, 71 (2013).
4 T. Egami, Ann. NY Acad. Sci. **371**, 238 (1981).
5 Y. T. Sun, R. Zhao, D. W. Ding, Y. H. Liu, H. Y. Bai, M. Z. Li, and W. H. Wang, Nat. Commun. **14**, 540 (2023).
6 Y. Sun, A. Concustell, and A. L. Greer, Nat. Rev. Mater. **1**, 16039 (2016).
7 Q. Yang, S. X. Peng, Z. Wang, and H. B. Yu, Natl. Sci. Rev. **7**, 1896 (2020).
8 R. Casalini, and C. M. Roland, Phys. Rev. Lett. **102**, 035701 (2009).
9 S. V. Ketov, Y. H. Sun, S. Nachum, Z. Lu, A. Checchi, A. R. Beraldin, H. Y. Bai, W. H. Wang, D. V. Louzguine-Luzgin, M. A. Carpenter, and A. L. Greer, Nature **524**, 200 (2015).
10 J. Pan, Y. P. Ivanov, W. H. Zhou, Y. Li, and A. L. Greer, Nature **578**, 559 (2020).
11 Y. H. Meng, S. Y. Zhang, W. H. Zhou, J. H. Yao, S. N. Liu, S. Lan, and Y. Li, Acta Mater. **241**, 118376 (2022).
12 A. D. Phan, A. Zaccone, V. D. Lam, and K. Wakabayashi, Phys. Rev. Lett. **126**, 025502 (2021).
13 X. Yuan, D. Şopu, F. Spieckermann, K. K. Song, S. V. Ketov, K. G. Prashanth, and J. Eckert, Script. Mater. **212**, 114575 (2022).
14 G. Ding, C. Li, A. Zaccone, W. H. Wang, H. C. Lei, F. Jiang, Z. Ling, and M. Q. Jiang, Sci. Adv. **5**, eaaw6249 (2019).
15 L. T. Zhang, Y. J. Wang, E. Pineda, Y. Yang, and J. C. Qiao, Int. J. Plast. **157**, 103402 (2022).

16 K. W. Park, C. M. Lee, M. Wakeda, Y. Shibutani, M. L. Falk, and J. C. Lee, Acta Mater. **56**, 5440 (2008).
17 A. L. Greer, and Y. H. Sun, Philos. Mag. **96**, 1643 (2016).
18 Z. Y. Zhou, H. L. Peng, and H. B. Yu, J. Chem. Phys. **150**, 204507 (2019).
19 Z. Y. Zhou, Y. Sun, L. Gao, Y. J. Wang, and H. B. Yu, Acta Mater. **246**, 118701 (2023).
20 Q. Sun, D. M. Miskovic, H. Kong, and M. Ferry, Appl. Surf. Sci. **546**, 149048 (2021).
21 W. Jiang, and B. Zhang, J. Appl. Phys. **127**, 115104 (2020).
22 A. L. Greer, and F. Spaepen, Ann. NY Acad. Sci. **371**, 218 (1981).
23 J. C. Ye, J. Lu, C. T. Liu, Q. Wang, and Y. Yang, Nat. Mater. **9**, 619 (2010).
24 E. Pineda, P. Bruna, B. Ruta, M. Gonzalez-Silveira, and D. Crespo, Acta Mater. **61**, 3002 (2023).
25 Y. Duan, L. Zhang, J. Qiao, Y. J. Wang, Y. Yang, T. Wada, H. Kato, J. Pelletier, E. Pineda, and D. Crespo, Phys. Rev. Lett. **129**, 175501 (2022).
26 T. J. Lei, L. R. DaCosta, M. Liu, W. H. Wang, Y. H. Sun, A. L. Greer, and M. Atzmon, Acta Mater. **164**, 165 (2019).
27 L. T. Zhang, Y. J. Duan, D. Crespo, E. Pineda, Y. J. Wang, J. M. Pelletier, and J. C. Qiao, Sci. China-Phys. Mech. Astron. **64**, 296111 (2021).
28 Y. R. Gao, Y. Tong, L. J. Song, X. X. Shui, M. Gao, J. T. Huo, and J. Q. Wang, Script. Mater. **224**, 115114 (2023).
29 Y. Q. Cheng, and E. Ma, Prog. Mater. Sci. **56**, 379 (2011).
30 P. Ross, S. Küchemann, P. M. Derlet, H. B. Yu, W. Arnold, P. Liaw, K. Samwer, and R. Maaß, Acta Mater. **138**, 111 (2017).
31 G. V. Afonin, Y. P. Mitrofanov, A. S. Makarov, N. P. Kobelev, W. H. Wang, and V. A. Khonik, Acta Mater. **115**, 204 (2016).
32 V. A. Khonik, K. Kitagawa, and H. Morii, J. Appl. Phys. **87**, 8440 (2000).
33 S.-J. Lee, B.-G. Yoo, J.-I. Jang, and J. C. Lee, Met. Mater. Int. **14**, 9 (2008).
34 S. C. Lee, C. M. Lee, J. W. Yang, and J. C. Lee, Script. Mater. **58**, 591 (2008).
35 S. C. Lee, C. M. Lee, J. C. Lee, H. J. Kim, Y. Shibutani, E. Fleury, and M. L. Falk, Appl. Phys. Lett. **92**, 151906 (2008).
36 K. W. Park, C. M. Lee, M. Wakeda, Y. Shibutani, E. Fleury, and J. C. Lee, Script. Mater. **59**, 710 (2008).
37 F. Mear, B. Lenk, Y. Zhang, and A. Greer, Script. Mater. **59**, 1243 (2008).
38 H. S. Chen, Appl. Phys. Lett. **29**, 328 (1976).
39 A. Revesz, E. Schafler, and Z. Kovacs, Appl. Phys. Lett. **92**, 011910 (2008).
40 J. J. Lewandowski, and A. L. Greer, Nat. Mater. **5**, 15 (2006).
41 D. Fiocco, G. Foffi, and S. Sastry, Phys. Rev. Lett. **112**, 025702 (2014).
42 J. C. Qiao, L. T. Zhang, Y. Tong, G. J. Lyu, Q. Hao, and K. Tao, Adv. Mech. **52**, 117 (2022).
43 M. B. Costa, J. J. Londoño, A. Blatter, A. Hariharan, A. Gebert, M. A. Carpenter, and A. L. Greer, Acta Mater. **244**, 118551 (2023).
44 L. Zhang, Y. Wang, Y. Yang, and J. Qiao, Sci. China-Phys. Mech. Astron. **65**, 106111 (2022).
45 G. Ding, F. Jiang, X. Song, L. H. Dai, and M. Q. Jiang, Sci. China-Phys. Mech. Astron. **65**, 264613 (2022).
46 L. T. Zhang, Y. J. Wang, Y. Yang, and J. C. Qiao, J. Mater. Sci. Tech. **158**, 53 (2023).